CFD-PBM coupled simulation of a nanobubble generator with honeycomb structure

PAPER • OPEN ACCESS

CFD-PBM coupled simulation of a nanobubble generator with honeycomb structure

To cite this article: F Ren *et al* 2018 *IOP Conf. Ser.: Mater. Sci. Eng.* **372** 012012

View the article online for updates and enhancements.

Related content

- Photomedicine and Stem Cells: PBM and dental stem cells
  H Abrahamse and M R Hamblin

- Design and performance of honeycomb structure for nanobubbles generating apparatus having different cell dimensions
  T Ueda, H F Zhai, F Ren et al.

- Development of an aquaculture system using nanobubble technology for the optimation of dissolved oxygen in culture media for nile tilapia (*Oreochromis niloticus*)
  G Mahasri, A Saskia, P S Apandi et al.

CFD-PBM coupled simulation of a nanobubble generator with honeycomb structure

F Ren[1], N A Noda[1,3], T Ueda[1], Y Sano[1], Y Takase[1], T Umekage[1], Y Yonezawa[2] and H Tanaka[1]

[1]Mechanical Engineering Department, Kyushu Institute of Technology, 1-1 Sensui-cho, Tobata-ku, Kitakyushu-shi, 804-8550, Japan
[2]Mrufukusuisan Corp., Ltd., 94-22 Nishiminato-machi, Kokurakita-ku, Kitakyushu-shi, 803-0801, Japan

E-mail: noda@mech.kyutech.ac.jp

Abstract. In recent years, nanobubble technologies have drawn great attention due to their wide applications in many fields of science and technology. The nitrogen nanobubble water circulation can be used to slow the progressions of oxidation and spoilage for the seafood long-term storage. From previous studies, a kind of honeycomb structure for high-efficiency nanobubble generation has been proposed. In this paper, the bubbly flow in the honeycomb structure was studied. The numerical simulations of honeycomb structure were performed by using a computational fluid dynamics–population balance model (CFD-PBM) coupled model. The numerical model was based on the Eulerian multiphase model and the population balance model (PBM) was used to calculate the gas bubble size distribution. The bubble coalescence and breakage were included. Considering the effect of bubble diameter on the fluid flow, the phase interactions were coupled with the PBM. The bubble size distributions in the honeycomb structure under different work conditions were predicted. The experimental results were compared with the simulation predictions.

1. Introduction

Recently, a kind of honeycomb structure was designed for high-efficiency nanobubble generation [1]. The aggregation and breakage happen and cause a wide range bubble size distribution when the bubbles flow in the honeycomb structure. Calculation of the bubble size and number density distribution and understanding of the bubble aggregation and breakage in bubbly flow are very important for the evaluation and improvement of the nanobubble generating ability.

Nowadays, many researches on gas-liquid flows have been carried out with computational fluid dynamics (CFD) simulations for engineering purposes [2]. The Euler–Lagrange (E-L) approach [3,4] and the Euler–Euler (E-E) approach [5,6] are primarily used. And the population balance method is a well-known method for tracking the size distribution of the dispersed phase and accounting for the breakage and coalescence effects in bubbly flows [7,8]. This approach is concerned with maintaining a record of the number of bubbles initially and tracking their evolution in space over time.

A progress in the CFD simulation of bubbly flow is the coupling of the population balance model (PBM) into CFD models, namely the CFD-PBM coupled model [2,9-11]. CFD-PBM coupled model combines the PBM into the CFD framework so that bubble breakup and coalescence can be taken into account, beneficial for describing the bubble size distribution and gas holdup in different flow regimes,

and it also considers the influence of bubble size on the interphase interaction, which allows it to well predict the local gas-liquid interfacial area and the flow behavior in diverse flow regimes [12].

In this work, the CFD-PBM coupled model along with the RNG k-ε turbulence model was used to simulate the bubble aggregation and breakage and predict the bubble number density distribution for the case of gas-liquid bubbly flow in the honeycomb structure under different work conditions.

2. Model descriptions

2.1. Euler–euler two-fluid model

For the bubbly flow in the honeycomb structure, the liquid is treated as a continuous primary phase and the gas as a dispersed secondary phase. The main continuity and momentum conservation equations for the liquid and gas phases are given as follows,

$$\frac{\partial}{\partial t}\left(\alpha_q\rho_q\right) + \nabla\cdot\left(\alpha_q\rho_q\vec{u}_q\right) = 0 \tag{1}$$

where α_q, ρ_q and $\vec{u}_q$ are the volume fraction, density and velocity of the qth phase respectively. The momentum balance for the qth phase is

$$\frac{\partial}{\partial t}\left(\alpha_q\rho_q\vec{u}_q\right) + \nabla\cdot\left(\alpha_q\rho_q\vec{u}_q\vec{u}_q\right) = -\alpha_q\nabla p + \nabla\cdot\overline{\tau}_q + \alpha_q\rho_q\vec{g} + \vec{F}_{drag,\ q} + \vec{F}_{lift,\ q} + \vec{F}_{VM,\ q} \tag{2}$$

where $\overline{\tau}_q$, p and $\vec{g}$ are the qth phase stress-strain tensor, pressure and gravity acceleration respectively. $\vec{F}_{drag,\ q}$ is the drag force, $\vec{F}_{lift,\ q}$ is the lift force and $\vec{F}_{VM,\ q}$ is the virtual mass force acting on the qth phase.

The RNG-based k-ε turbulence model [13] is derived from the instantaneous Navier-Stokes equations, using a mathematical technique called "renormalization group" (RNG) methods. It has greater potential to give accurate predictions for complex flows. The k and ε for continuous phase are computed by the follows,

$$\frac{\partial}{\partial t}\left(\alpha_q\rho_q k_q\right) + \nabla\cdot\left(\alpha_q\rho_q\vec{u}_q k_q\right) = \nabla\cdot\left(\alpha_q\left(\mu_q + \frac{\mu_{t,q}}{\sigma_k}\right)\nabla k_q\right) + \alpha_q G_{k,q} - \alpha_q\rho_q\varepsilon_q \tag{3}$$

and

$$\frac{\partial}{\partial t}\left(\alpha_q\rho_q\varepsilon_q\right) + \nabla\cdot\left(\alpha_q\rho_q\vec{u}_q\varepsilon_q\right) = \nabla\cdot\left(\alpha_q\left(\mu_q + \frac{\mu_{t,q}}{\sigma_\varepsilon}\right)\nabla\varepsilon_q\right) + \alpha_q\frac{\varepsilon_q}{k_q}\left(C_{1\varepsilon}G_{k,q} - C_{2\varepsilon}\rho_q\varepsilon_q\right) \tag{4}$$

In these equations, σ_k and σ_ε are the turbulent Prandtl numbers for k and ε, respectively. $C_{1\varepsilon}$ and $C_{2\varepsilon}$ are constants. $G_{k,q}$ is the production of turbulent kinetic energy.

2.2. Discrete population balance model

Assuming the gas phase to be made of spherical bubbles of diameter L, the dispersed phase volume fraction can be expressed as

$$\alpha_p(\vec{x},t) = \int_0^{+\infty} n(\vec{x},\Phi,t)\frac{\pi}{6}L^3 dL \tag{5}$$

The bubble state vector is characterized by a set of external coordinates *(x)* which denote the spatial position of the bubble and *(Φ)* is referred to as an internal coordinate which could include particle size, composition, and temperature. $n(\vec{x},\Phi,t)$ is the number density function. Assuming that Φ is the bubble volume, the transport equation for $n(\vec{x},\Phi,t)$ can be given as

$$\frac{\partial}{\partial t}[n(V,t)] + \nabla\cdot[\vec{u}n(V,t)] = B_{ag}(V,t) + B_{br}(V,t) - D_{ag}(V,t) - D_{br}(V,t) \tag{6}$$

The terms $B_{ag}(V,t)$, $B_{br}(V,t)$, $D_{ag}(V,t)$, $D_{br}(V,t)$ represent birth due to aggregation, birth due to breakage, death due to aggregation, and death due to breakage, respectively.

## 3. Nanobubble generating device and experimental details

From previous studies, a kind of honeycomb structure for high-efficiency nanobubble generation was proposed. Figure 1 shows the bubble generating device equipped with several parallel honeycomb structure units. The water and nitrogen gas are pumped into the bubble generator together as is shown in figure 1(a). There are 15 honeycomb structure units placed in parallel inside the bubble generator as is shown in figure 1(b). Figure 2 shows the details of the honeycomb structure unit. One honeycomb unit consists of two honeycomb structure plates stacked so that the complex crisscross flow channels are formed in the honeycomb unit.

(a) Experimental device   (b) Parallel honeycomb units
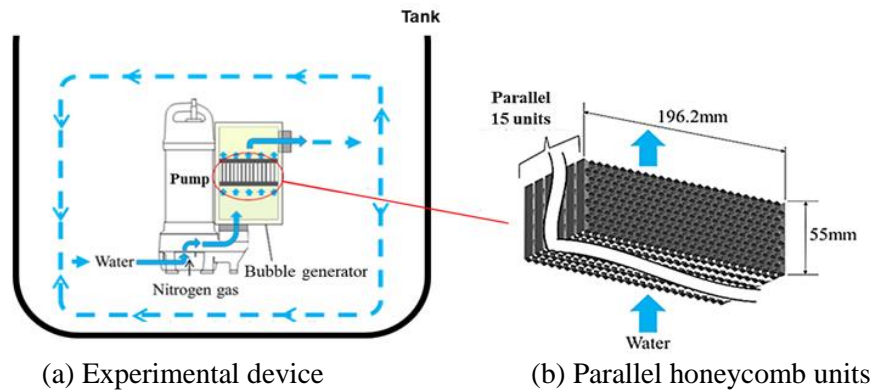
Figure 1. Nitrogen nanobubble generating device.

(a) Honeycomb unit composition   (b) Honeycomb unit cross section
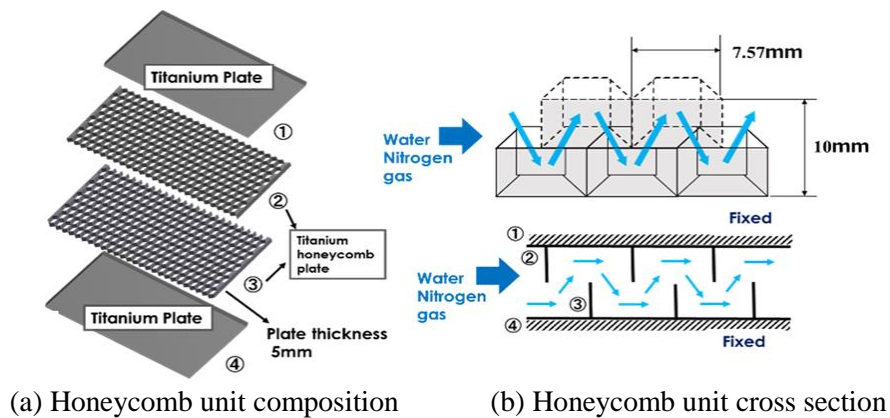
Figure 2. Honeycomb structure.
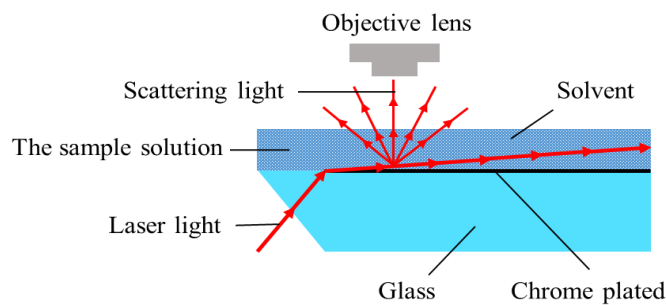
Figure 3. Schematic of Nano Sight LM10-HS.

The nanobubble density in the tank is measured from the sample taken from the tank. The nano-particle analyzer, Nano Sight LM10-HS [14,15], is used to measure the nanobubble density of the sample. Figure 3 shows the principle of Nano Sight LM10-HS. Irradiating a laser beam in the horizontal direction in the sample liquid, the side-scattered light from the nanoparticles is visualized by the objective lens, the movement trajectory of each particle is displayed on the computer. Tracking Brownian motion of all particles recognized on the screen and using the Stokes-Einstein equation, the particle size is obtained from the moving velocity of the particle.

The details of the experimental device are shown in table 1. The main purpose of the bubble generating device is to reduce the dissolved oxygen (DO) in the water by using the nitrogen nanobubbles. The experimental results of different flow rates are shown in table 2. In the experiment, the flow rate of the gas-liquid mixture is controlled by the pump power, and the gas flow rate is a constant 5 L/min. From table 2, it can be seen that the DO decreases and the particle number density increases over the time. It should be noted that not all of the particles are nitrogen nanobubbles because it is hard to distinguish what type of a particle might be. However, it can be inferred that most of the increased particles are the nitrogen bubbles generated by the device, and these bubbles make the DO lower. It can be also found that the device can generate more bubbles with higher flow rate. The bubble size and number density distribution will be analyzed in the next chapter.

Table 1. Details of the experimental device.

| Item	Specification
Pump	Submersible pump(80TM23.7)
Output [kW]	3.7, (60Hz)
Tank [mm]	1580×1100×600
Water and amount [kg]	Tap water, 1000
Gas	Nitrogen
Flow rate [L/min]	5.0

Table 2. Experimental results of DO.

| Time	Flow rate 700 L/min		Flow rate 550 L/min	
	DO [mg/L]	Particle number density [x10^8/mL]	DO [mg/L]	Particle number density [x10^8/mL]
0min	10.4	0.37	10.14	0.41
10min	4.4	0.82	7.79	0.43
20min	2.5	1.12	6.7	0.88
30min	1.7	1.72	5.5	0.94

4. Numerical details

In this work, all computations were performed by using the commercial CFD software FLUENT 16.2. Because of the symmetry, only a part of one honeycomb structure unit will be modeled to simplify the CFD analysis, as is shown in figure 4. According to the device in the experiment, the length of the side of the hexagon is 3.5 mm and the thickness of the wall between two hexagons is 0.5 mm. Pressure-outlet boundary condition is applied. Along the walls, no-slip boundary conditions are adopted. The symmetry boundary conditions are applied on the two sides of the model. The inlet velocities are 0.456 m/s and 0.358 m/s according to the flow rates 700 L/min and 550 L/min. An assumption is that the gas phase has the same velocity as the liquid phase at the inlet because the gas volume fraction is small and the bubble size is small. The number of bubble bins is specified 10, from 10 nm to 5200 nm. It is assumed that all the bubbles at the inlet have the diameter 1280 nm initially.

Figure 5 shows the bubble number density distributions of different flow rates at the inlet and outlet. Due to the fixed gas flow rate 5 L/min, the gas volume fraction is smaller when the flow rate is high, the bubble number density when the flow rate is 700 L/min is smaller than that when the flow

rate is 550 L/min. It can be found that most of the bubbles at the inlet aggregate into larger bubbles after flowing through the honeycomb structure. The bubble breakage in the bubbly flow is not as obvious as the aggregation. Figure 6 shows the number density distribution of the bubbles with size less than 350 nm at the outlet. It can be seen that more small bubbles are generated when the flow rate is 700 L/min.
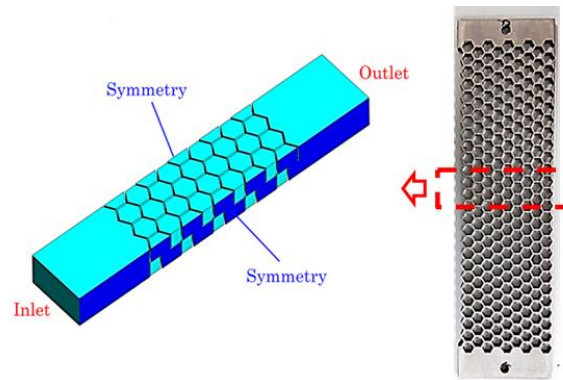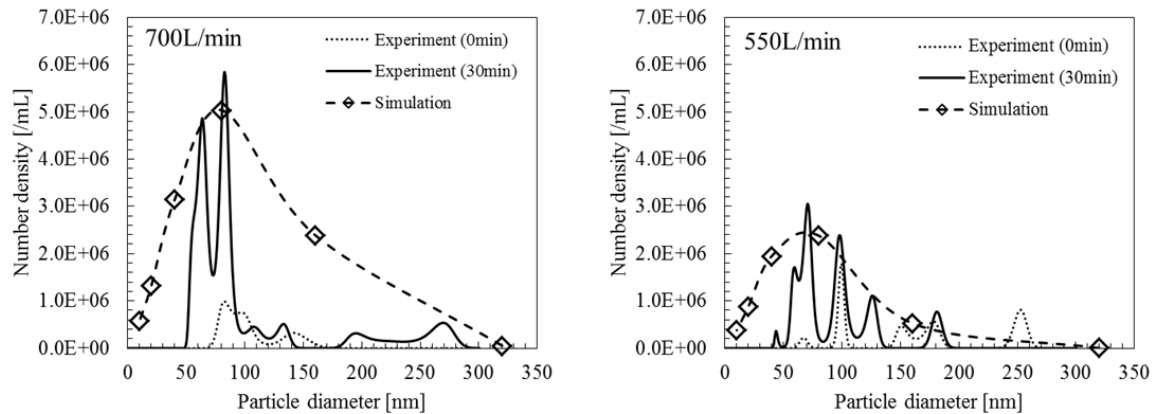

Figure 4. Simplified honeycomb unit model.
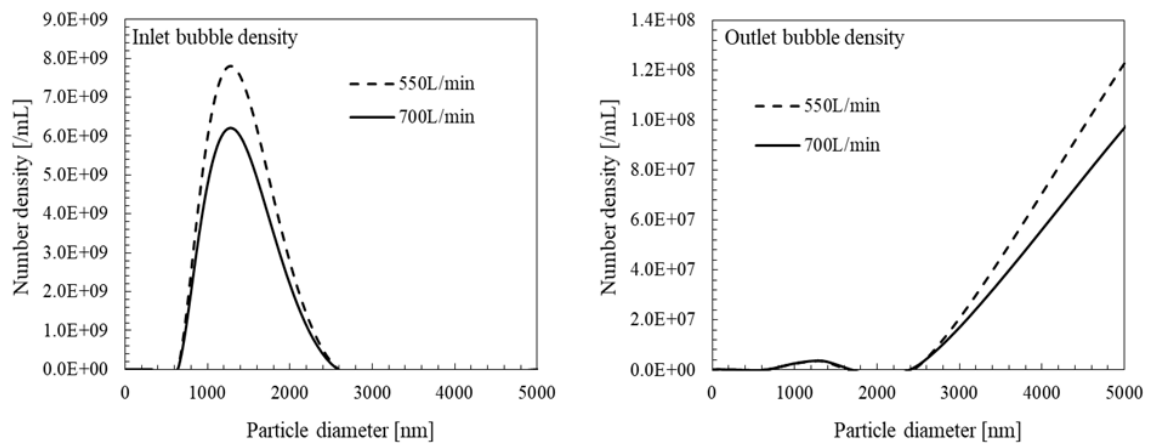
Figure 5. The bubble number density distribution of different flow rates.
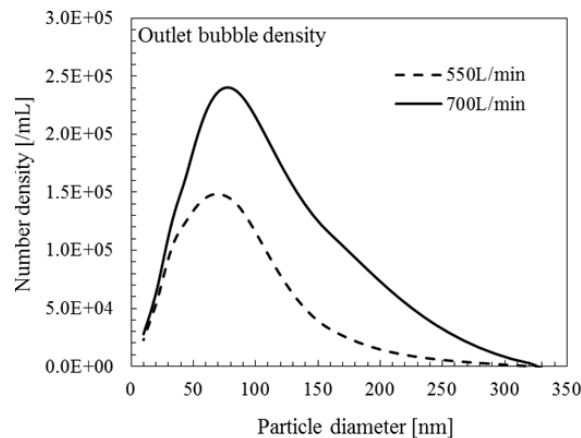
Figure 6. The number density distribution of the bubbles with size less than 350 nm.

Figure 7. The bubble number density distribution in the tank.

The large bubbles in the tank quickly rise to the surface of water and collapse, only the tiny bubbles remain in the water tank and are detected by Nano Sight LM10-HS. Figure 7 shows the bubble number density distribution in the tank. The simulation result is obtained by

$$N_{pbm}^{tank} = \frac{N_{pbm}^{outlet} \cdot Q_{total} \cdot t}{V_{water}^{tank}} \tag{7}$$

where N_{pbm}^{outlet} is the number density at the outlet as is shown in figure 6, Q_{total} is the flow rate (550L/min or 700 L/min), t is the experiment time (30 min) and V_{water}^{tank} is the volume of water in the tank (1 m³). N_{pbm}^{tank} denotes the number density of the bubbles generated from the device, the original particles in the water tank when t=0min are not included. The 30-minute experimental result includes the original particles. In figure 7, the simulation result can approximately reflect the trend of number density distribution. In the range of 0nm to 350 nm, only 6 bin sizes are calculated because of the limit of computer power, the more accurate solution can be obtained by calculating more bubble bins using more computing resource. In the experiment, the number of bubbles with diameter of 70 nm is the largest when the flow rate is 550 L/min, the number of bubbles with diameter of 82 nm is the largest when the flow rate is 700 L/min. Table 3 shows the number densities of the bubbles with diameters of 70 nm and 82 nm. Simulation results are obtained by interpolation from the results of 6 bin sizes shown in figure 7. The original particles should not be counted so that the effective number density can be calculated by subtracting the 0-minute experimental result from the 30-minute experimental result. It can be found in Table 3 that the simulation result can accurately predict what bubble size is predominant in the water tank. As shown in figure 7, only 6 bin sizes are calculated in the range of 0 nm to 350 nm, and their number densities are shown in table 4. The results of these 6 bins do not coincide with the experimental results very well, however, in figure 7 it can be seen that the curve of these 6 bins can be used to predict the trend of number density distribution.

Table 3. Number density details of the bubbles with diameters of 70 nm and 82 nm.

		Flow rate 550 L/min Bubble size 70 nm	Flow rate 700 L/min Bubble size 82 nm
Experimental result	0 min	96727/mL	989257/mL
	30 min	3056609/mL	5843111/mL
	30 min-0 min	2959882/mL	4853854/mL
Simulation result		2608186/mL	4999691/mL
Error		12%	2%

Table 4. Number density details of 6 bins.

Bin size [nm]	Flow rate 550 L/min			Flow rate 700 L/min		
	Experimental result (0 min) [/mL]	Experimental result (30 min) [/mL]	Simulation result [/mL]	Experimental result (0 min) [/mL]	Experimental result (30 min) [/mL]	Simulation result [/mL]
320	0	0	1891	0	0	52733
160	204324	186	527698	90351	57	2394528
80	941	213412	2382769	931425	5019031	5036182
40	0	364302	1950508	0	0	3142667
20	0	0	880177	0	0	1317974
10	0	0	376941	0	0	582056

5. Conclusions

In this work, the bubble aggregation and breakage processes in bubbly flow in honeycomb structure were studied. From the results of simulation and experiment, most of the nitrogen bubbles aggregate into the larger bubbles and get out of the water quickly. Few bubbles become the tiny bubbles and remain in the water. The gas utilization rate is not very high, however, it is still a simple and effective way to increase the gas content in water. This kind of honeycombed generator also has the advantages of simple structure, easy assembly and production, low requirements for use and maintenance, and large quantity of bubbles for wide applications.

The bubble aggregation and breakage in turbulence were simulated by using the CFD-PBM coupled model along with the RNG k-ε turbulence model. The bubble number density distribution was predicted. Comparing with the experimental results, the simulation results can approximately reflect the trend of number density distribution and accurately predict the predominant bubble size in the water tank. The more accurate solution of the number density distribution can be obtained by calculating more bubble bins using more computing resource.

References

[1]   Kudo Y and Hiraki K 2011 Characteristics comparison of the honeycomb mixing device by considering the mixing energy in the gas-liquid mixing *The Proceedings of the Symposium on Micro-Nano Science and Technology* **3** 26-7

[2]   Liang X F, Pan H, Su Y H and Luo Z H 2016 CFD-PBM approach with modified drag model for the gas-liquid flow in a bubble column *Chem. Eng. Res. Des.* **112** 88-102

[3]   Delnoij E, Lammers F, Kuipers J and Van Swaaij W 1997 Dynamic simulation of dispersed gas-liquid two-phase flow using a discrete bubble model *Chem. Eng. Sci.* **52** 1429–58

[4]   Sokolichin A, Eigenberger G, Lapin A and Lübert A 1997 Dynamic numerical simulation of gas-liquid two-phase flows Euler/Euler versus Euler/Lagrange *Chem. Eng. Sci.* **52** 611–26

[5]   Drew D 1983 Mathematical modeling of two-phase flow *Annu. Rev. Fluid. Mech.* **15** 261–91

[6]   Krishna R, Urseanu M I, van Baten J M and Ellenberger J 1999 Influence of scale on the hydrodynamics of bubble columns operating in the churn-turbulent regime: experiments vs. eulerian simulations *Chem. Eng. Sci.* **54** 4903–11

[7]   Wang T F, Wang J F and Jin Y 2005 Population balance model for gas−liquid flows: influence of bubble coalescence and breakup models *Ind. Eng. Chem. Res.* **44** 7540-9

[8]   Li L M, Liu Z Q, Li B K, Matsuura H and Tsukihashi F 2015 Water model and CFD-PBM coupled model of gas-liquid-slag three-phase flow in ladle metallurgy *ISIJ. Int.* **55** 1337-4

[9]   Duan X Y, Cheung S C P, Yeoh G H, Tu J Y, Krepper E and Lucas D 2011 Gas–liquid flows in medium and large vertical pipes *Chem. Eng. Sci.* **66** 872–83

[10] Wang T and Wang J 2007 Numerical simulations of gas-liquid mass transfer in bubble columns with a CFD–PBM coupled model *Chem. Eng. Sci.* **62** 7107–18

[11] Wang T, Wang J and Jin Y 2006 A CFD-PBM coupled model for gas-liquid flows *Am. Ins.Chem. Eng. J.* **52** 125–40

[12]   Xing C, Wang T and Wang J 2013 Experimental study and numerical simulation with a coupled CFD–PBM model of the effect of liquid viscosity in a bubble column *Chem. Eng. Sci.* **95** 313–22

[13]   Yakhot V, Orszag S A, Thangam S, Gatski T B and Speziale C G 1992 Development of turbulence models for shear flows by a double expansion technique *Phys. Fluids. A.* **4** 1510-20

[14]   Malloy A and Carr B 2006 Nanoparticle tracking analysis *Part. Part. Syst. Char.* **23** 197-204

[15]   Filipe V, Hawe A and Jiskoot W 2010 Critical evaluation of Nanoparticle Tracking Analysis (NTA) by NanoSight for the measurement of nanoparticles and protein aggregates *Pharm. Res.* **27** 796-810